

From Particles to Fields: Reframing Photon Mapping with Continuous Gaussian Photon Fields

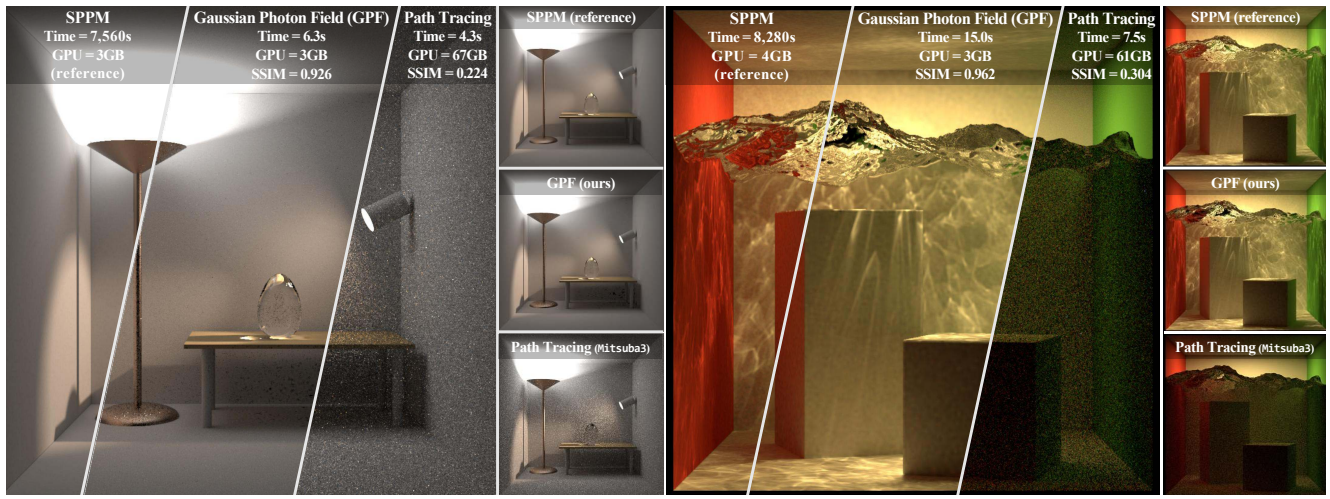
Jiachen Tao^{1,2,†}Yuchun Liu²Meng Zheng²Weitai Kang¹Benjamin Planche^{2,‡}Haoxuan Wang¹Feiran Wang¹Terrence Chen²Van Nguyen Nguyen^{2,‡}Zhongpai Gao²Anwesa Choudhuri²Yan Yan¹Junyi Wu^{1,2,†}Gengyu Zhang¹Zhenghao Zhao¹Ziyan Wu²¹University of Illinois Chicago, Chicago, IL, USA²United Imaging Intelligence, Boston, MA, USA

Figure 1. **Gaussian Photon Field (GPF)** unifies photon mapping and neural field representations, achieving physically accurate, efficient, and view-reusable global illumination across diverse scenes, including indirect lighting (left) and water caustics (right). Using *Stochastic Progressive Photon Mapping (SPPM)* [12] as reference, our method produces substantially higher structural similarity (SSIM) compared to the *Mitsuba 3 Path Tracer* [16], while reducing rendering costs by orders-of-magnitude compared to SPPM.

Abstract

Accurately modeling light transport is essential for realistic image synthesis. Photon mapping provides physically grounded estimates of complex global illumination effects such as caustics and specular-diffuse interactions, yet its per-view radiance estimation remains computationally inefficient when rendering multiple views of the same scene. The inefficiency arises from independent photon tracing and stochastic kernel estimation at each viewpoint, leading to inevitable redundant computation. To accelerate multi-view rendering, we reformulate photon mapping as a continuous and reusable radiance function. Specifically, we introduce the **Gaussian Photon Field (GPF)**, a learnable representation that encodes photon distributions as anisotropic 3D Gaussian primitives parameterized by position, rotation, scale, and spectrum. GPF is initialized from physically traced photons in the first SPPM iteration and optimized using multi-view supervision of final radiance, distilling photon-based light transport into a continuous field. Once trained, the field enables differentiable radiance evaluation along camera rays without repeated photon tracing or iterative refinement. Extensive experiments on scenes with complex light transport, such as caustics and specular-diffuse interactions, demonstrate that GPF attains photon-level accuracy while reducing computation by orders of magnitude, unifying the physical rigor of photon-based rendering with the efficiency of neural scene representations.

[†]This work was carried out during the internship of Jiachen Tao and Junyi Wu at United Imaging Intelligence, Boston MA, USA.

[‡]Corresponding authors.

1. Introduction

Accurately modeling light transport [20] is fundamental to realistic image synthesis, with applications in interactive graphics [4, 21, 47], medical imaging simulation [8, 34, 39], scene understanding via inverse graphics [1, 2, 49], *etc.* Physically-based rendering techniques [9, 37], such as photon mapping [18] and its variants [12, 13, 23], have long served as reliable estimators for complex global illumination, effectively capturing challenging phenomena such as caustics, indirect reflections, and refractions. Despite their accuracy, these methods remain computationally expensive when rendering multiple views of the same scene.

Prior work on photon mapping [18] addresses complex global illumination by decoupling light transport into two stochastic processes: photon tracing and density estimation. During photon tracing, photons emitted from light sources are stored upon surface and volumetric interactions, forming a global photon map. In the subsequent density estimation stage, the radiance at visible points is reconstructed by gathering nearby photons using spatial averaging based on stochastic kernel density estimation (KDE) [19, 35]. This formulation enables accurate estimation of caustics and diffuse inter-reflections, making photon mapping a robust estimator for a wide range of lighting phenomena.

However, photon mapping is fundamentally ill-suited for multi-view rendering. While photon tracing is view-agnostic and the photon map can be reused, storing millions or billions of photons is often impractical. More importantly, the radiance-gathering step is inherently view-dependent [12, 13, 18], requiring recomputation for each camera view. The kernel density estimate introduces view-dependent bias, as each view gathers a different subset of photons, causing flickering, brightness shifts, or blur. Increasing photon density reduces variance but raises memory and computation costs. Thus, the tight coupling between visibility and per-view estimation makes classical photon mapping accurate but inefficient for multi-view reuse.

In contrast, modern neural scene representations, *e.g.* neural radiance fields (NeRF) [28] and 3D Gaussian splatting (3DGS) [22], represent scene appearance and geometry as continuous functions that can be queried from arbitrary viewpoints. By learning such a shared representation, these methods amortize rendering costs across views. This motivates a fundamental question: **can photon mapping, traditionally a discrete, view-dependent estimator be reformulated as a continuous radiance field that encodes photon distributions throughout the scene?** Such a formulation would enable consistent photon reuse across views, preserving the physical accuracy of photon mapping while achieving neural-style efficiency.

Toward this goal, we introduce the **Gaussian Photon Field (GPF)**, a learnable radiance representation that unifies photon mapping and neural field paradigms. GPF mod-

els the global photon distribution as a set of anisotropic 3D Gaussian primitives, each parameterized by its position, rotation, scale, and spectrum, forming a continuous and differentiable radiance field that can be queried from arbitrary viewpoints. Unlike traditional 3D Gaussian splatting, which represents view-dependent surface appearance, GPF encodes view-independent photon distributions that capture global light transport phenomena such as caustics and indirect illumination. Once optimized, GPF enables efficient radiance evaluation along camera rays to render novel views, eliminating the need for repeated photon tracing, stochastic density estimation, or progressive refinement as in standard photon mapping. Conceptually, GPF replaces per-view KDE with a single, continuous photon-based radiance field.

We construct and optimize our Gaussian Photon Field in three stages: (1) Initialization: Gaussian primitives are initialized from photons traced in a single iteration of stochastic progressive photon mapping (SPPM) [12], providing a physically grounded starting point; (2) Radiance Query: a differentiable mechanism aggregates contributions from nearby Gaussians to estimate surface radiance, triggered at the first diffuse intersection after any specular or glossy bounces, at which point the ray terminates; (3) Supervision: the field is optimized end-to-end against reference radiance computed offline by SPPM, using sparse multi-view supervision. This process distills complex, view-dependent light transport into a continuous, reusable radiance field.

To validate the effectiveness of our approach, we conduct extensive experiments across multiple physically challenging scenes, including complex caustic and specular-diffuse interactions. We compare Gaussian Photon Field against classical physically-based integrators, *e.g.*, path tracing [16] and SPPM [12], as well as other learnable solutions, *e.g.*, NeRF [28] and 3DGS [22]. Measuring visual quality, render time, and storage cost, results confirm that GPF achieves photon-level accuracy with significantly reduced computational redundancy and successfully unifies the physical accuracy of photon-based rendering with the efficiency and scalability of continuous learned representations.

2. Related Work

Physically-Based Global Illumination. Simulating global illumination (GI) [20] is a central problem in computer graphics. Unbiased Monte Carlo methods, such as path tracing (PT) [20] and its bidirectional variants (BDPT) [37], are considered the gold standard for accuracy. However, they struggle to efficiently sample complex, low-probability light paths, such as those that form caustics, often resulting in high variance and noise.

To address this, biased techniques like photon mapping [18] and its stochastic progressive variant SPPM [12] were developed. As detailed in Sec. 3, these methods ex-

cel at capturing complex GI phenomena by decoupling light transport into a two-pass process. Their primary limitation, however, is the *per-view estimation paradigm*, which fundamentally relies on a view-dependent kernel density estimation (KDE) process that must be re-executed for every new camera view. Our work directly targets this bottleneck, as illustrated in Figure 2, instead of proposing a new sampling strategy for these methods, we reformulate their core estimation process, replacing the repeated, per-view KDE with a query to a persistent, continuous radiance function.

Neural and Learned Scene Representations. The concept of a continuous, learnable scene representation was popularized by neural radiance fields (NeRF) [28]. NeRF and its many successors [5, 11, 25–27, 31–33, 36, 42, 43] achieve state-of-the-art novel view synthesis. However, these methods are essentially “black-box” appearance models: optimized for view interpolation, they lack physical grounding and cannot guarantee accurate light transport for complex effects such as caustics or relighting.

More recently, 3D Gaussian splatting (3DGS) [14, 22, 46] has achieved remarkable success, combining the efficiency of explicit primitives with the representational quality of neural scene models for real-time appearance reconstruction. We draw inspiration from 3DGS in its use of Gaussians as a compact and expressive primitive. However, our approach differs fundamentally in both objective and rendering pipeline. While 3DGS focuses on modeling scene appearance and geometry through a differentiable rasterization (splatting) process, our photon field models the scene’s global illumination and radiance distribution arising from physical light transport. As shown in Figure 2, instead of rasterizing Gaussians to reproduce appearance, we employ them within a differentiable ray-tracing framework, where radiance is computed through continuous field queries. Our GPF thus extends the expressive power of Gaussian primitives to a physically-grounded domain, enabling efficient and reusable estimation of global illumination across views.

Radiance Caching and Density Learning. Radiance caching techniques [24, 41] interpolate illumination from sparsely sampled shading points to reduce variance and speed up rendering. While effective for single frames, these caches are transient and view-dependent, needing reconstruction for each new view. Our method builds a persistent, view-independent radiance representation, amortizing light transport across all views.

Gaussian mixture models (GMM) [6, 10, 15, 38, 44, 45, 50] have also been used to approximate light transport. Jakob *et al.* [15] fit a compact anisotropic GMM to volumetric photon distributions, providing a parametric approximation for accelerated volumetric radiance queries. In their formulation, Gaussians act as statistical surrogates of photon density, obtained through progressive EM and used to

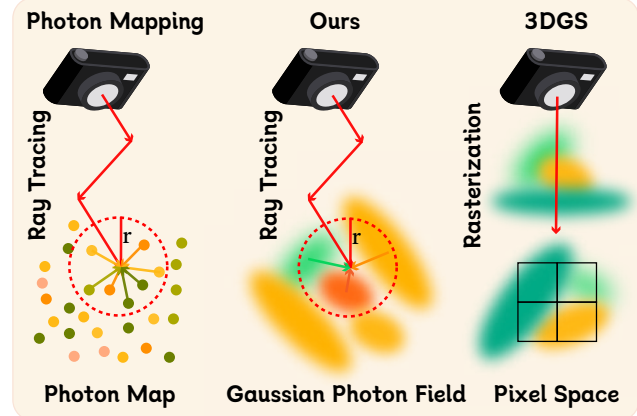


Figure 2. **Comparison of rendering processes.** Classical photon mapping estimates radiance by gathering discrete photons within a local radius r during ray tracing. Our GPF replaces this with a continuous, differentiable photon field queried via ray tracing. In contrast, 3DGS rasterizes Gaussian primitives in pixel space, emphasizing appearance over physically grounded light transport.

replace kernel-based density estimation in volumetric photon mapping. In contrast, our method does not fit or compress a photon map. We only use a single SPPM iteration to initialize a set of Gaussian primitives with a physically meaningful prior. These primitives are then fully optimized in radiance space, supervised by multi-view radiance reference, and no longer correspond to structure in the photon map. Consequently, GPF serves as a view-independent radiance field representation, rather than a statistical acceleration structure, bridging photon-based global illumination with differentiable radiance-field modeling.

3. Preliminaries

Our work bridges classical light transport simulation with modern, learnable representations. To formally ground our method, we first review the rendering equation and then summarize the mathematics of progressive photon mapping—the paradigm we aim to reformulate.

3.1. Rendering Equation

Physically-based rendering aims to solve the rendering equation [20], a formulation of light transport in equilibrium. It states that the outgoing radiance L_o from a surface point \mathbf{x} in a direction ω_o is the sum of its emitted light L_e and all reflected incoming light:

$$L_o(\mathbf{x}, \omega_o) = L_e(\mathbf{x}, \omega_o) + \int_{\Omega} f_r(\mathbf{x}, (\omega_o)) L_i(\mathbf{x}, \omega_i) (\mathbf{n} \cdot \omega_i) d\omega_i, \quad (1)$$

where f_r is the bidirectional reflectance distribution function (BRDF) [30] describing the material, \mathbf{n} is the surface normal, Ω is the hemisphere of all incoming directions ω_i , and L_i is the incoming radiance at \mathbf{x} from direction ω_i .

The primary challenge in rendering is solving for L_i , as it is the solution to another rendering equation at the next surface intersection. This recursive integral is particularly difficult to solve for complex light paths, such as caustics, where high-energy contributions from a light source are focused onto a diffuse surface after interacting with a specular (e.g., glass or metal) surface. Unidirectional Monte Carlo methods, e.g., path tracing [20], struggle to sample these low-probability paths efficiently, leading to high variance.

3.2. Stochastic Progressive Photon Mapping

Photon mapping [18] and its progressive variants [12, 13] were introduced specifically to solve these difficult light paths. SPPM reformulates the problem by decoupling light transport into two passes.

Pass 1: Photon Tracing. In a view-independent pass, photons are traced from light sources and stored upon interacting with non-specular surfaces. Each photon p records its position \mathbf{x}_p and flux $\Delta\Phi_p$. These photons are organized in a global spatial structure, such as a k-d tree or hash grid, forming the photon map for subsequent density estimation.

Pass 2: Radiance Estimation. In a view-dependent pass, radiance is computed at all visible surface points $\{\mathbf{x}\}$ for the current camera. SPPM performs this estimation using iterative kernel density estimation. In each iteration k , a search radius r_k is used to find nearby photons. The radiance is estimated by summing the flux of all N_p photons within the radius and normalizing by the kernel area:

$$L_i(\mathbf{x}) \approx \frac{1}{\pi r_k^2} \sum_{p=1}^{N_p} \Delta\Phi_p. \quad (2)$$

This radiance estimate is progressively refined by simultaneously tracing more photons (increasing N_p) and shrinking the radius r_k , which allows the estimate to converge to a physically accurate result.

Crucially, this estimation process of gathering photons at a visible point and managing its local radius, is fundamentally coupled to the camera view. It underpins the **per-view estimation paradigm** that limits photon mapping, whereas our method replaces with a continuous, reusable function.

4. Method

4.1. Gaussian Photon Field Representation

Our method begins by recasting the discrete particle set of SPPM into a continuous, differentiable representation. Instead of a sparse point cloud, we introduce a Gaussian photon field (GPF), defined as a mixture of N anisotropic 3D Gaussian primitives, $\{\mathcal{G}_i\}_{i=1}^N$. Each primitive is parameterized as $\mathcal{G}_i = (\boldsymbol{\mu}_i, \mathbf{q}_i, \mathbf{s}_i, \Phi_i)$, with a mean position $\boldsymbol{\mu}_i \in \mathbb{R}^3$, a rotation $\mathbf{q}_i \in \mathbb{H}$ (represented as a unit quaternion), a scale $\mathbf{s}_i \in \mathbb{R}_+^3$, and a spectral flux $\Phi_i \in \mathbb{R}^3$. The rotation and

scale collectively define the anisotropic covariance matrix $\boldsymbol{\Sigma}_i$. The radiance contribution G_i of a single primitive at any 3D point \mathbf{x} is then given by its un-normalized, flux-weighted Gaussian function:

$$G_i(\mathbf{x}) = \Phi_i \exp \left[-\frac{1}{2} (\mathbf{x} - \boldsymbol{\mu}_i)^\top \boldsymbol{\Sigma}_i^{-1} (\mathbf{x} - \boldsymbol{\mu}_i) \right]. \quad (3)$$

A key component of our method is its **physically-inspired initialization**. The GPF is not created from scratch, but directly seeded from classical simulation. We run a single iteration of SPPM to trace and store a sparse photon map. For each of the N photons p in this map, we instantiate one Gaussian primitive \mathcal{G}_i , mapping the physical properties directly. The Gaussian mean is set to the photon's surface position: $\boldsymbol{\mu}_i \leftarrow \mathbf{x}_p$, and the Gaussian flux is set to the photon's flux: $\Phi_i \leftarrow \Delta\Phi_p$. Rotation \mathbf{q}_i and scale \mathbf{s}_i have no direct analog in a discrete particle. We therefore randomly initialize \mathbf{q}_i and set the initial \mathbf{s}_i to a small, isotropic value, providing diverse local support for subsequent optimization. Through gradient-based optimization, orientations and scales will align with dominant light paths. This *particle-to-field* process (illustrated in Figure 3) results in a continuous, differentiable field, setting the stage for gradient-based optimization and efficient, reusable radiance queries.

4.2. Differentiable Radiance Querying

During training and inference, rendering proceeds by tracing camera rays through the scene for radiance estimation, querying the Gaussian photon field, which encodes the spatial distribution of photon energy. This design replaces discrete photon-based estimation with a continuous radiance function, allowing radiance to be evaluated directly from the learned Gaussian field without repeated tracing. This section describes our hybrid ray tracing pipeline (Sec. 4.2.1) and the radiance query mechanism (Sec. 4.2.2).

4.2.1. Ray Tracing with Gaussian Radiance Integration

We employ a path-tracing-style camera integrator augmented with Gaussian radiance field queries for diffuse interactions. Given a camera ray $\mathbf{r}(t) = \mathbf{o} + t\mathbf{d}$, the outgoing radiance is computed by the rendering equation:

$$L_o(\mathbf{x}, \omega_o) = L_e(\mathbf{x}, \omega_o) + \int_{\Omega} f_r(\mathbf{x}, (\omega_i)) L_i(\mathbf{x}, \omega_i) |\cos \theta_i| d\omega_i, \quad (4)$$

where $L_i(\mathbf{x}, \omega_i)$ is approximated by $L_{\text{GPF}}(\mathbf{x}, \omega_i)$.

Our algorithm follows the standard path-tracing loop but introduces a key modification at diffuse interactions. When a view ray first encounters a diffuse surface, instead of spawning further secondary rays or gathering photons, we query GPF to obtain the preaccumulated incident radiance. This hybrid design drastically reduces variance and avoids double-counting BSDF contributions, as the radiance stored

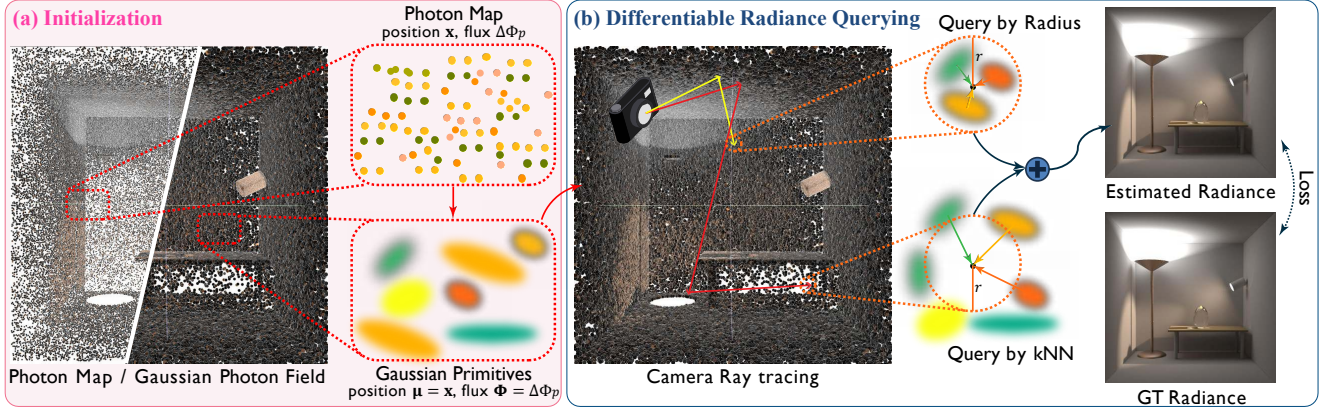


Figure 3. **Overview of the Gaussian Photon Field (GPF) pipeline.** (a) **Initialization.** We convert the discrete photon map from one SPPM iteration into a continuous Gaussian photon field by instantiating one anisotropic 3D Gaussian per photon. Each primitive inherits the photon’s position and flux, with rotation and scale randomly initialized. (b) **Differentiable radiance querying.** During training and rendering, camera rays are traced through the scene. At the first diffuse intersection, radiance is estimated by aggregating contributions from nearby Gaussians via a radius-based and k-nearest-neighbor query. The predicted radiance is supervised by the GT values at corresponding surface points, enabling end-to-end optimization of all Gaussian parameters and producing a differentiable, view-reusable radiance field.

in the field already encodes the expected reflected contribution from photon sampling during optimization. The accumulated radiance at a diffuse surface point \mathbf{x} is thus:

$$L(\mathbf{x}) = L_e(\mathbf{x}) + \beta L_{\text{GPF}}(\mathbf{x}), \quad (5)$$

where β denotes the current throughput. For specular or glossy interactions, we continue the path tracing:

$$\beta \leftarrow \beta \cdot \frac{f_r(\mathbf{x}, (\omega_o)) |\cos \theta_i|}{p(\omega_o)}. \quad (6)$$

This hybrid formulation preserves physical correctness for specular transport while amortizing diffuse transport via the learned Gaussian radiance. As shown in Figure 3, camera rays propagate through the scene: specular and glossy bounces use classical path tracing, while diffuse bounces query the Gaussian field for fast radiance estimation.

4.2.2. Radiance Query and Aggregation

Given a surface query point \mathbf{x} (first diffuse hit) with outgoing direction ω_o toward the viewer, we gather contributions from a spatial neighborhood $\mathcal{N}(\mathbf{x})$ of nearby Gaussians. The GPF aggregated radiance is computed as

$$L_{\text{GPF}}(\mathbf{x}, \omega_o) = \sum_{i \in \mathcal{N}(\mathbf{x})} w_i(\mathbf{x}) \Phi_i, \quad (7)$$

The spatial weight $w_i(\mathbf{x})$ is an anisotropic Gaussian kernel modulated by a smooth distance falloff:

$$w_i(\mathbf{x}) = \exp\left(-\frac{1}{2} (\mathbf{x} - \boldsymbol{\mu}_i)^\top \boldsymbol{\Lambda}_i (\mathbf{x} - \boldsymbol{\mu}_i)\right) \cdot \psi(\|\mathbf{x} - \boldsymbol{\mu}_i\|), \quad (8)$$

with $\psi(\cdot)$ a soft attenuation that decays near a maximum radius r_{\max} , to ensure stability and avoid hard boundaries.

The BSDF term f_r modulates the field query by the surface reflectance properties, ensuring that Gaussian primitives Φ_i encode a base radiance field that is view-independent, while the final radiance L_{GPF} correctly accounts for directional reflectance. All terms are differentiable w.r.t. $(\boldsymbol{\mu}_i, \mathbf{q}_i, \mathbf{s}_i, \Phi_i)$, enabling end-to-end optimization.

Neighborhood Search. To balance efficiency and adaptivity, we employ a hybrid spatial retrieval strategy:

$$\mathcal{N}(\mathbf{x}) = \text{BallQuery}(\mathbf{x}, r) \cup \text{kNN}(\mathbf{x}, \max(0, k_{\min} - k_r)). \quad (9)$$

I.e., for dense photon regions, we perform a radius-based query using a KD-tree (BallQuery), returning k_r Gaussians. In sparse regions, where $k_r < k_{\min}$ neighbors are found, we supplement with a k-nearest-neighbor (kNN) query to guarantee coverage. This ensures consistent density support while maintaining smooth transitions.

Differentiable Accumulation. All components of the query—including anisotropic weighting, soft distance attenuation, and normalization—are differentiable with respect to the Gaussian parameters $(\boldsymbol{\mu}, \mathbf{q}, \mathbf{s}, \Phi)$. We implement the computation in a vectorized manner on the GPU using Dr. Jit [17], and aggregate per-neighborhood contributions via a parallel scatter-reduce. This design enables efficient batched training and stable gradient-based optimization and supports fast radiance evaluation once the field is trained, without relying on non-differentiable lookups or per-view kernel density estimation.

4.3. Supervision and Training

The Gaussian photon field is trained under sparse multi-view supervision derived from physically-based progressive photon mapping [12]. Instead of supervising at the image level, we supervise at the level of *first-bounce diffuse sur-*

Table 1. **Quantitative comparison across five physically-based rendering scenes.** We report PSNR, SSIM, LPIPS, and storage cost (in MB). The **best** (red), the **second best** (orange) results are highlighted.

Method	Veach-Bidir				Veach-Ajar				Water-Caustic			
	PSNR↑	SSIM↑	LPIPS↓	Storage↓	PSNR↑	SSIM↑	LPIPS↓	Storage↓	PSNR↑	SSIM↑	LPIPS↓	Storage↓
Path Tracer 10 spp	16.01	0.134	0.778	–	9.276	0.098	0.651	–	12.09	0.221	0.663	–
Path Tracer 50 spp	19.90	0.224	0.716	–	15.21	0.242	0.531	–	12.86	0.319	0.573	–
SPPM - 3 it	18.01	0.146	0.696	26.49	14.58	0.314	0.516	405.3	26.53	0.664	0.413	14.16
GPF (Ours)	37.61	0.926	0.338	18.33	25.84	0.691	0.324	267.2	27.12	0.936	0.158	9.724
Water-Caustic 2				Cornell Box				Mean				
Method	PSNR↑	SSIM↑	LPIPS↓	Storage↓	PSNR↑	SSIM↑	LPIPS↓	Storage↓	PSNR↑	SSIM↑	LPIPS↓	Storage↓
Path Tracer 10 spp	11.88	0.248	0.637	–	30.49	0.654	0.497	–	15.95	0.271	0.645	–
Path Tracer 50 spp	12.24	0.304	0.579	–	34.59	0.850	0.403	–	18.96	0.388	0.560	–
SPPM - 3 it	25.64	0.632	0.412	16.26	30.47	0.754	0.399	21.63	23.05	0.502	0.487	96.77
GPF (Ours)	28.72	0.962	0.196	12.34	39.73	0.936	0.183	15.46	31.80	0.890	0.240	64.61

face points—that is, the surface intersections where camera rays first encounter diffuse materials. This design ensures precise geometric alignment between the queried radiance and the ground-truth locations, while excluding background and invalid samples.

Ground-truth Generation. For each of the k training camera views, we gather the set of diffuse surface points visible from the camera: $\mathcal{V} = \{\mathbf{x}_i \in \mathcal{D} \mid \exists \gamma \in \mathcal{P}(o, \mathbf{x}_i) : \text{NonDiffuse}(\gamma, \mathcal{S} \setminus \mathcal{D}) \wedge \text{FirstDiffuse}(\gamma, \mathcal{D})\}$, where o is the camera position, \mathcal{S} is the full scene geometry, $\mathcal{D} \subset \mathcal{S}$ is the diffuse subset, and $\mathcal{P}(o, \mathbf{x})$ denotes the set of all finite piecewise-linear paths from o to \mathbf{x} . The predicate $\text{NonDiffuse}(\gamma, \mathcal{S} \setminus \mathcal{D})$ is true if each intermediate point of γ lies on a non-diffuse surface, including both specular and glossy interactions, and $\text{FirstDiffuse}(\gamma, \mathcal{D})$ is true if the path first intersects a diffuse point at its endpoint.

For every supervision point $\mathbf{x} \in \mathcal{V}$, the ground-truth radiance is computed using a high-quality Stochastic Progressive Photon Mapping (SPPM) reference. Although generating these references is computationally expensive, it is performed only once for training; once optimized, our field enables fast, reusable radiance queries for arbitrary novel views. Following the standard SPPM procedure, photons are traced from light sources and stored only on diffuse surfaces during each iteration. The radiance at \mathbf{x} is then estimated by photon gathering across multiple progressive iterations, and the final ground-truth value is obtained by averaging the per-iteration results:

$$L_{\text{ref}}(\mathbf{x}, \omega_o) = \frac{1}{N_{\text{iter}}} \sum_{t=1}^{N_{\text{iter}}} L_t(\mathbf{x}, \omega_o), \quad (10)$$

where each iteration L_t computes radiance by gathering nearby photons and evaluating the BSDF [12, 30]:

$$L_t(\mathbf{x}, \omega_o) = \frac{1}{\pi r_t^2} \sum_{\mathbf{p}_i \in \mathcal{B}_t(\mathbf{x})} \Phi_i \cdot f_r(\mathbf{x}, (\omega_o)), \quad (11)$$

with ω_i denoting the photon incident direction, ω_o the camera viewing direction, $\mathcal{B}_t(\mathbf{x})$ the photon neighborhood within radius r_t , and Φ_i the photon power. This yields a low-variance, physically-accurate estimate of the directional outgoing radiance at \mathbf{x} .

Training. During optimization, we trace camera rays for the same k reference views and query the photon field at each *first diffuse surface intersection* to obtain predicted radiance $L_{\text{GPF}}(\mathbf{x})$. The field parameters are optimized by minimizing a mean-squared error (MSE) loss in radiance space:

$$\mathcal{L}_{\text{MSE}} = \frac{1}{|\mathcal{V}|} \sum_{\mathbf{x} \in \mathcal{V}} \|L_{\text{GPF}}(\mathbf{x}, \omega_o) - L_{\text{ref}}(\mathbf{x}, \omega_o)\|_2^2. \quad (12)$$

5. Experiments

We validate our method on our newly-proposed challenging benchmark, comparing to both classical physically-based integrators and standard neural rendering approaches and justifying design choices via multiple ablation studies.

5.1. Experimental Setup

Datasets. Since no standard or well-established datasets exist for this task, we propose a new one consisting of five physically-based rendering scenes that cover a wide range of light-transport phenomena, including specular–diffuse interactions, caustics, and glossy reflections:

- *Veach-Bidir* and *Veach-Ajar*: classic Mitsuba-3-compatible test scenes from Bitterli’s rendering resources [3], featuring multi-bounce specular–diffuse paths and complex indirect illumination.
- *Water-Caustic* and *Water-Caustic 2*: scenes inspired by Bitterli [3] and reconfigured for Mitsuba 3, focusing on challenging refractive and specular-diffuse caustics.
- *Cornell Box* [16]: canonical diffuse reference scene to evaluate radiometric accuracy and convergence behavior.

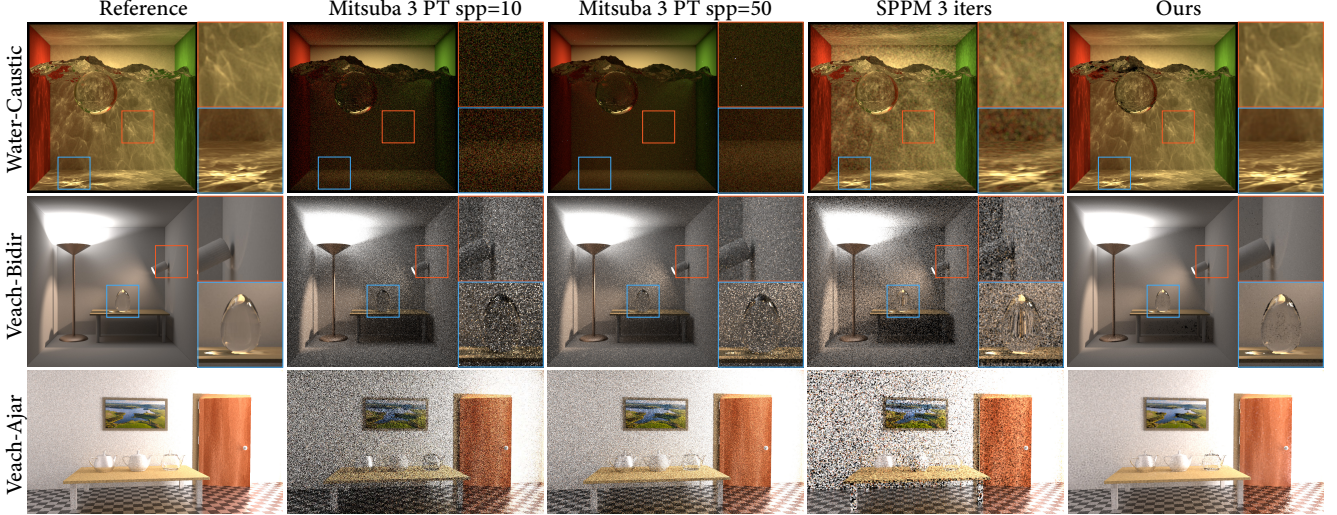


Figure 4. **Qualitative comparison results.** We compare our solution with *Mitsuba 3 Path Tracer* and *SPPM* across scenes with complex indirect illumination and caustics. Our method produces cleaner results with significantly fewer noise artifacts and more accurate light transport, especially in challenging caustic and multi-bounce diffuse regions. Please zoom in for more details.

Table 2. **Rendering time (s) comparison across five scenes.**

Method	V-Bidir	V-Ajar	W-Caustic	W-Caustic 2	Cornell
PT 10 spp	3.9	3.8	3.7	3.9	2.5
PT 50 spp	4.3	5.0	7.4	7.5	4.5
SPPM - 3 iters	23.4	42.0	26.4	24.7	32.8
SPPM - 1000 iters	7,793.3	14,010.0	8,790.0	8246.7	10,923.0
GPF (Ours)	6.3	30.1	16.34	15.3	26.7

Training Protocol. For the *Veach-Bidir* scene, GPF is trained on 30 views using per-pixel final radiance from SPPM. For the other scenes, the model relies on only 3 views. Radiance maps are rendered at a resolution of 720×1280 for *Veach-Ajar*, and 1024×1024 for the rest.

5.2. Quantitative Results

Comparison with Integrators. In Table 1, we compare GPF with several physically-based integrators across five representative scenes. *Path tracer* corresponds to the default integrator in *Mitsuba 3* [16], while *stochastic progressive photon mapping (SPPM)* is our own standard implementation built upon the same framework.

The results show that GPF achieves the highest overall performance across all metrics (PSNR [7], SSIM [40], LPIPS [48]). In scenes dominated by indirect lighting (*Veach-Bidir*, *Veach-Ajar*), our method significantly surpasses all baselines in both SSIM and LPIPS, demonstrating its ability to capture smooth, high-frequency radiance variations while maintaining global consistency. For caustic-dominated scenes (*Water-Caustic*, *Water-Caustic 2*), GPF achieves the best PSNR and substantially outperforms others in SSIM and LPIPS, highlighting its capacity to accurately model concentrated photon energy distributions through the learned continuous field. While PSNR is a

Table 3. **Comparison with Instant-NGP [29] and 3DGS [22].** We use caustic scenes and different numbers of training views. The **best**, the **second best** results are highlighted.

Method	Water-Caustic			Water-Caustic 2		
	PSNR↑	SSIM↑	LPIPS↓	PSNR↑	SSIM↑	LPIPS↓
INGP - 3 views	13.42	0.466	0.748	13.09	0.460	0.734
INGP - 10 views	12.59	0.473	0.618	12.44	0.480	0.620
3DGS - 3 views	16.76	0.508	0.493	17.80	0.550	0.485
3DGS - 10 views	26.58	0.812	0.246	26.44	0.843	0.244
GPF (Ours)	27.12	0.936	0.158	28.72	0.962	0.196

pixel-wise metric sensitive to small local deviations, our method preserves perceptual and structural fidelity much better, as reflected by large gains in SSIM and LPIPS. Even on the simple *Cornell Box*, GPF consistently outperforms all baselines across metrics, confirming its robustness and general applicability to diverse light transport phenomena.

Table 2 compares the rendering time per image across all five scenes. While the Path Tracer (spp=10 and spp=50) provides fast but noisy results, and SPPM - 3 iters yields moderate accuracy at the cost of higher computation, our Gaussian Photon Field achieves comparable visual quality to the SPPM - 1000 iters reference while being orders of magnitude faster. Specifically, SPPM - 1000 iters—used only for generating the reference and final radiance ground truth—requires several hours per frame (up to 14,000 seconds), whereas GPF produces results of similar fidelity within only 6–30 seconds per image. This efficiency stems from reusing the learned radiance field across views, eliminating repeated photon tracing and progressive iterations.

Comparison with Neural Radiance Fields. In Table 3, we further compare our method with neural rendering ap-

Figure 5. **Multi-view comparison on Water-Caustic 2 with NeRF and 3DGS.** Unlike NeRF and 3DGS, which exhibit view-dependent artifacts under sparse supervision, Gaussian Photon Field (GPF) preserves consistent caustics and global illumination even with 3 views.

Table 4. **Ablation study on different components.**

w_{init}	w_{radius}	w_{knn}	PSNR \uparrow	SSIM \uparrow	LPIPS \downarrow
	✓		26.73	0.8962	0.2152
		✓	26.42	0.8847	0.2118
	✓	✓	26.90	0.9026	0.2208
✓	✓		26.93	0.9128	0.1792
✓		✓	26.97	0.9118	0.1769
✓	✓	✓	27.12	0.9355	0.1579

proaches, including Instant-NGP [29] and 3D Gaussian splatting (3DGS) [22], trained under both sparse (3 views) and dense (10 views) supervision. While Instant-NGP and 3DGS are trained only with RGB images and camera parameters, our GPF additionally leverages geometry, material, and lighting information during training. To make comparison more reasonable, we supervise GPF only with 3-view final radiance maps on the *Water-Caustic* and *Water-Caustic 2* scenes. GPF consistently surpasses all baselines on both scenes, achieving the highest PSNR, SSIM, and lowest LPIPS. While 3DGS-10views improves notably over sparse-view settings, its performance remains below GPF even though GPF uses only limited supervision. This highlights GPF’s superior ability to reconstruct physically consistent caustics and high-frequency illumination, benefiting from its photon-based initialization and differentiable radiance query. Unlike purely neural methods that learn view-dependent appearance, GPF maintains global illumination coherence across views, producing both higher numerical accuracy and visually stable results.

Ablation Studies. Table 4 analyzes the influence of three key components in our framework: the physically grounded initialization (w_{init}), the radius-based neighborhood weighting (w_{radius}), and the k -nearest-neighbor fallback (w_{knn}). Without initialization, Gaussian primitives are randomly sampled, and the lack of photon-based priors makes optimization unstable, often leading to suboptimal local minima. Using only w_{radius} leaves sparse regions without valid Gaussians, resulting in incomplete radiance reconstruction. Using only w_{knn} removes spatial adaptivity, producing over-

smoothed illumination and weaker caustics. Combining all three components yields the best performance: w_{init} provides a stable physical prior, w_{radius} ensures spatial adaptivity, and w_{knn} offers a robust fallback in sparse regions. Further ablation studies are provided in the appendix.

5.3. Qualitative Results

Figure 4 presents qualitative comparisons across three representative scenes, with more exhaustive results in supplementary material. For the *Water-Caustic* scene, GPF produces sharp, accurate caustics that capture the subtle refractive patterns, while *SPPM - 3 iters* yields blurred illumination due to its limited photon budget and the *Mitsuba 3 Path Tracer* fails to recover detailed structures even at 50 spp. In the *Veach-Bidir* scene, which features complex multi-bounce diffuse transport and glossy interreflections, GPF achieves a clean, noise-free reconstruction with well-defined highlights, unlike *SPPM - 3 iters* and the *Path Tracer*, which exhibit noise and structural artifacts. Similarly, in the *Veach-Ajar* scene, GPF provides smooth, stable illumination with accurate indirect lighting, whereas other integrators suffer from high-frequency noise and incomplete light transport. Overall, GPF combines the physical accuracy of photon-based rendering with the smoothness of a continuous learned radiance field, delivering superior results for both caustic and indirect illumination.

Furthermore, as shown in Figure 5, our photon field enables strong consistency across novel viewpoints. Despite large changes in camera pose and viewing direction, both direct and indirect lighting remain coherent, with stable caustics and diffuse shading. This highlights the robustness and view-reusability of our learned radiance field, effectively amortizing photon-based light transport across views. Additional per-view visualizations for all scenes are provided in the supplementary material.

6. Conclusion

We introduced the Gaussian Photon Field (GPF), a physically grounded radiance representation that unifies

photon mapping and neural fields. By reformulating per-view kernel density estimation into a continuous Gaussian field, GPF enables efficient, view-reusable global illumination while preserving physical accuracy. Experiments show that GPF achieves photon-level accuracy with orders-of-magnitude faster rendering and strong multi-view consistency. This formulation bridges classical light transport simulation and learnable radiance representations, pointing toward physically accurate, differentiable rendering of dynamic and volumetric scenes.

References

- [1] Dejan Azinovic, Tzu-Mao Li, Anton Kaplyan, and Matthias Nießner. Inverse path tracing for joint material and lighting estimation. In *Proceedings of the IEEE/CVF Conference on Computer Vision and Pattern Recognition*, pages 2447–2456, 2019. [2](#)
- [2] Jonathan T Barron and Jitendra Malik. Shape, illumination, and reflectance from shading. *IEEE Transactions on Pattern Analysis and Machine Intelligence*, 37(8):1670–1687, 2014. [2](#)
- [3] Benedikt Bitterli. Rendering resources, 2016. <https://benedikt-bitterli.me/resources/>. [6](#)
- [4] Benedikt Bitterli, Chris Wyman, Matt Pharr, Peter Shirley, Aaron Lefohn, and Wojciech Jarosz. Spatiotemporal reservoir resampling for real-time ray tracing with dynamic direct lighting. *ACM Transactions on Graphics (TOG)*, 39(4):148–1, 2020. [2](#)
- [5] Ting-Hsuan Chen, Jie Wen Chan, Hau-Shiang Shiu, Shih-Han Yen, Changhan Yeh, and Yu-Lun Liu. Narcan: Natural refined canonical image with integration of diffusion prior for video editing. In *Advances in Neural Information Processing Systems (NeurIPS)*, 2024. [3](#)
- [6] Jorge Condor, Sébastien Speierer, Lukas Bode, Aljaz Bozic, Simon Green, Piotr Didyk, and Adrian Jarabo. Don’t splat your gaussians: Volumetric ray-traced primitives for modeling and rendering scattering and emissive media. *ACM Transactions on Graphics (TOG)*, 44(1):1–17, 2025. [3](#)
- [7] A. M. Eskicioglu and P. S. Fisher. Image quality measures and their performance. *IEEE Transactions on Communications*, 43(12):2959–2965, 1995. [7](#)
- [8] Qianqian Fang and David A Boas. Monte carlo simulation of photon migration in 3d turbid media accelerated by graphics processing units. *Optics express*, 17(22):20178–20190, 2009. [2](#)
- [9] Cindy M. Goral, Kenneth E. Torrance, Donald P. Greenberg, and Bennett Battaile. Modeling the interaction of light between diffuse surfaces. In *Proceedings of the 11th Annual Conference on Computer Graphics and Interactive Techniques*, page 213–222, New York, NY, USA, 1984. Association for Computing Machinery. [2](#)
- [10] Paul Green, Jan Kautz, Wojciech Matusik, and Frédéric Durand. View-dependent precomputed light transport using nonlinear gaussian function approximations. In *Proceedings of I3D*, 2006. [3](#)
- [11] Xiang Guo, Jiadai Sun, Yuchao Dai, Guanying Chen, Xiaozheng Ye, Xiao Tan, Errui Ding, Yumeng Zhang, and Jingdong Wang. Forward flow for novel view synthesis of dynamic scenes, 2023. [3](#)
- [12] Toshiya Hachisuka and Henrik Wann Jensen. Stochastic progressive photon mapping. *ACM Transactions on Graphics (TOG)*, 28(5):1–8, 2009. [1](#), [2](#), [4](#), [5](#), [6](#), [3](#)
- [13] Toshiya Hachisuka, Shinji Ogaki, and Henrik Wann Jensen. Progressive photon mapping. *ACM Transactions on Graphics (TOG)*, 27(5), 2008. [2](#), [4](#)
- [14] Binbin Huang, Zehao Yu, Anpei Chen, Andreas Geiger, and Shenghua Gao. 2d gaussian splatting for geometrically accurate radiance fields. In *Special Interest Group on Computer Graphics and Interactive Techniques Conference Conference Papers ’24*, page 1–11. ACM, 2024. [3](#)
- [15] Wenzel Jakob, Christian Regg, and Wojciech Jarosz. Progressive Expectation–Maximization for hierarchical volumetric photon mapping. *Computer Graphics Forum*, 30(4), 2011. [3](#)
- [16] Wenzel Jakob, Sébastien Speierer, Nicolas Roussel, Merlin Nimier-David, Delio Vicini, Tizian Zeltner, Baptiste Nicolet, Miguel Crespo, Vincent Leroy, and Ziyi Zhang. Mitsuba 3 renderer, 2022. <https://mitsuba-renderer.org>. [1](#), [2](#), [6](#), [7](#), [3](#), [4](#), [5](#)
- [17] Wenzel Jakob, Sébastien Speierer, Nicolas Roussel, and Delio Vicini. Dr.jit: A just-in-time compiler for differentiable rendering. *Transactions on Graphics (Proceedings of SIGGRAPH)*, 41(4), 2022. [5](#), [1](#), [2](#)
- [18] Henrik Wann Jensen. Global illumination using photon maps. In *Proceedings of the Eurographics Workshop on Rendering Techniques ’96*, page 21–30, Berlin, Heidelberg, 1996. Springer-Verlag. [2](#), [4](#)
- [19] Henrik Wann Jensen. *Realistic image synthesis using photon mapping*. AK Peters/crc Press, 2001. [2](#)
- [20] James T. Kajiya. The rendering equation. In *Proceedings of the 13th Annual Conference on Computer Graphics and Interactive Techniques*, page 143–150, New York, NY, USA, 1986. Association for Computing Machinery. [2](#), [3](#), [4](#)
- [21] Alexander Keller. Instant radiosity. In *Proceedings of the 24th annual conference on Computer graphics and interactive techniques*, pages 49–56, 1997. [2](#)
- [22] Bernhard Kerbl, Georgios Kopanas, Thomas Leimkühler, and George Drettakis. 3d gaussian splatting for real-time radiance field rendering. *ACM Transactions on Graphics (TOG)*, 42(4), 2023. [2](#), [3](#), [7](#), [8](#), [4](#), [5](#)
- [23] Claude Knous and Matthias Zwicker. Progressive photon mapping: A probabilistic approach. *ACM Transactions on Graphics (TOG)*, 30(3), 2011. [2](#)
- [24] Jaroslav Křivánek, Pascal Gautron, Sumanta Pattanaik, and Kadi Bouatouch. Radiance caching for efficient global illumination computation. In *ACM SIGGRAPH 2008 Classes*, New York, NY, USA, 2008. Association for Computing Machinery. [3](#)
- [25] Zhengqi Li, Simon Niklaus, Noah Snavely, and Oliver Wang. Neural scene flow fields for space-time view synthesis of dynamic scenes. In *Proceedings of the IEEE/CVF Conference on Computer Vision and Pattern Recognition (CVPR)*, 2021. [3](#)

[26] Yu-Lun Liu, Chen Gao, Andreas Meuleman, Hung-Yu Tseng, Ayush Saraf, Changil Kim, Yung-Yu Chuang, Johannes Kopf, and Jia-Bin Huang. Robust dynamic radiance fields. In *Proceedings of the IEEE/CVF Conference on Computer Vision and Pattern Recognition (CVPR)*, 2023.

[27] Caoyuan Ma, Yu-Lun Liu, Zhixiang Wang, Wu Liu, Xinchen Liu, and Zheng Wang. Humannerf-se: A simple yet effective approach to animate humannerf with diverse poses. In *Proceedings of the IEEE/CVF Conference on Computer Vision and Pattern Recognition (CVPR)*, 2024. 3

[28] Ben Mildenhall, Pratul P Srinivasan, Matthew Tancik, Jonathan T Barron, Ravi Ramamoorthi, and Ren Ng. Nerf: Representing scenes as neural radiance fields for view synthesis. *Communications of the ACM*, 65(1):99–106, 2021. 2, 3

[29] Thomas Müller, Alex Evans, Christoph Schied, and Alexander Keller. Instant neural graphics primitives with a multiresolution hash encoding. *ACM Transactions on Graphics (TOG)*, 41(4):102:1–102:15, 2022. 7, 8, 3, 5

[30] Fred E Nicodemus. Directional reflectance and emissivity of an opaque surface. *Applied optics*, 4(7):767–775, 1965. 3, 6

[31] Keunhong Park, Utkarsh Sinha, Jonathan T. Barron, Sofien Bouaziz, Dan B. Goldman, Steven M. Seitz, and Ricardo Martin-Brualla. Nerfies: Deformable neural radiance fields. *arXiv preprint arXiv:2102.07064*, 2021. 3

[32] Keunhong Park, Utkarsh Sinha, Peter Hedman, Jonathan T. Barron, Sofien Bouaziz, Dan B. Goldman, Ricardo Martin-Brualla, and Steven M. Seitz. Hypernerf: A higher-dimensional representation for topologically varying neural radiance fields. *arXiv preprint arXiv:2106.13228*, 2021.

[33] Albert Pumarola, Enric Corona, Gerard Pons-Moll, and Francesc Moreno-Noguer. D-nerf: Neural radiance fields for dynamic scenes. In *Proceedings of the IEEE/CVF conference on computer vision and pattern recognition*, pages 10318–10327, 2021. 3

[34] David Sarrut, Thomas Baudier, Damian Borys, Ane Etxebeste, Hermann Fuchs, Jan Gajewski, Loïc Grevillot, Sébastien Jan, George C Kagadis, Han Gyu Kang, et al. The opengate ecosystem for monte carlo simulation in medical physics. *Physics in Medicine & Biology*, 67(18):184001, 2022. 2

[35] Bernard W Silverman. *Density estimation for statistics and data analysis*. Routledge, 2018. 2

[36] Edgar Tretschk, Ayush Tewari, Vladislav Golyanik, Michael Zollhöfer, Christoph Lassner, and Christian Theobalt. Non-rigid neural radiance fields: Reconstruction and novel view synthesis of a dynamic scene from monocular video. In *Proceedings of the IEEE/CVF International Conference on Computer Vision (ICCV)*, 2021. 3

[37] Eric Veach. *Robust monte carlo methods for light transport simulation*. PhD thesis, Stanford, CA, USA, 1998. AAI9837162. 2

[38] Jiří Vorba, Ondřej Karlík, Martin Šík, Tobias Ritschel, and Jaroslav Krivánek. On-line learning of parametric mixture models for light transport simulation. *ACM Transactions on Graphics (TOG)*, 33(4), 2014. 3

[39] Lihong Wang, Steven L Jacques, and Liqiong Zheng. Mcml—monte carlo modeling of light transport in multi-layered tissues. *Computer methods and programs in biomedicine*, 47(2):131–146, 1995. 2

[40] Z. Wang, A. C. Bovik, H. R. Sheikh, and E. P. Simoncelli. Image quality assessment: From error visibility to structural similarity. *IEEE Transactions on Image Processing (TIP)*, 13(4):600–612, 2004. 7

[41] Gregory J. Ward, Francis M. Rubinstein, and Robert D. Clear. A ray tracing solution for diffuse interreflection. In *Proceedings of the 15th Annual Conference on Computer Graphics and Interactive Techniques*, page 85–92, New York, NY, USA, 1988. Association for Computing Machinery. 3

[42] Chun-Hung Wu, Shih-Hong Chen, Chih-Yao Hu, Hsin-Yu Wu, Kai-Hsin Chen, Yu-You Chen, Chih-Hai Su, Chih-Kuo Lee, and Yu-Lun Liu. Denver: Deformable neural vessel representations for unsupervised video vessel segmentation. In *Proceedings of the IEEE/CVF Conference on Computer Vision and Pattern Recognition (CVPR)*, 2025. 3

[43] Wenqi Xian, Jia-Bin Huang, Johannes Kopf, and Changil Kim. Space-time neural irradiance fields for free-viewpoint video. In *Proceedings of the IEEE/CVF conference on computer vision and pattern recognition*, pages 9421–9431, 2021. 3

[44] Kun Xu, Wei-Lun Sun, Zhao Dong, Dan-Yong Zhao, Run-Dong Wu, and Shi-Min Hu. Anisotropic spherical gaussians. *ACM Transactions on Graphics (TOG)*, 32(6), 2013. 3

[45] Ling-Qi Yan, Miloš Hašan, Steve Marschner, and Ravi Ramamoorthi. Position-normal distributions for efficient rendering of specular microstructure. *ACM Transactions on Graphics (TOG)*, 35(4), 2016. 3

[46] Ziyi Yang, Xinyu Gao, Yangtian Sun, Yihua Huang, Xiaoyang Lyu, Wen Zhou, Shaohui Jiao, Xiaojuan Qi, and Xiaogang Jin. Spec-gaussian: Anisotropic view-dependent appearance for 3d gaussian splatting, 2024. Preprint. 3

[47] Aijia Zhang, Yan Zhao, and Shigang Wang. Illumination estimation for augmented reality based on a global illumination model. *Multimedia tools and applications*, 78(23):33487–33503, 2019. 2

[48] Richard Zhang, Phillip Isola, Alexei A Efros, Eli Shechtman, and Oliver Wang. The unreasonable effectiveness of deep features as a perceptual metric. In *Proceedings of the IEEE conference on computer vision and pattern recognition*, pages 586–595, 2018. 7

[49] Yuanqing Zhang, Jiaming Sun, Xingyi He, Huan Fu, Rongfei Jia, and Xiaowei Zhou. Modeling indirect illumination for inverse rendering. In *Proceedings of the IEEE/CVF Conference on Computer Vision and Pattern Recognition*, pages 18643–18652, 2022. 2

[50] Yang Zhou, Songyin Wu, and Ling-Qi Yan. Unified gaussian primitives for scene representation and rendering. *arXiv preprint arXiv:2406.09733*, 2024. 3

From Particles to Fields: Reframing Photon Mapping with Continuous Gaussian Photon Fields

Supplementary Material

In this supplementary material, we provide additional implementation details for reproducibility (Section A), our complete ablation study (Section B) and additional experimental results (Section C). We also include a supplementary video illustrating the multi-view rendering consistency of our Gaussian Photon Field across diverse scenes.

A. Implementation Details

We implement both our baseline *Stochastic Progressive Photon Mapping (SPPM)* [12] and the proposed *Gaussian Photon Field (GPF)* integrator within the *Mitsuba 3* [16] rendering framework, built upon the *Dr.Jit* differentiable runtime [17]. Both integrators share the same scene interface and BSDF/geometry infrastructure, allowing direct performance and quality comparison.

A.1. SPPM Integrator

Our baseline follows the standard formulation of stochastic progressive photon mapping [12] (Algorithm S1), consisting of alternating *photon tracing* and *camera ray tracing* stages. Each iteration emits N_p photons from all light sources and stores them in a KD-tree for radiance estimation. The photon radius r_t is updated after each iteration according to

$$r_{t+1} = r_t \sqrt{\frac{t + \alpha}{t + 1}}, \quad (13)$$

where $\alpha = 0.7$ controls the blending rate between old and new photon contributions. For the experiments, we run $T = 1000$ iterations to produce the ground-truth reference radiance L_{ref} .

A.2. GPF Integrator

The GPF integrator extends the SPPM pipeline by replacing the per-view kernel density estimation (KDE) stage with a continuous, learnable Gaussian Photon field. We initialize a set of $M = N_p = 100,000$ anisotropic Gaussian primitives from the first SPPM iteration's photon map, using the photon position as the mean μ_i , initial scale $s_i = 0.01$, and random orientation \mathbf{q}_i . Each Gaussian stores the photon flux Φ_i as its radiance contribution.

During training, camera rays are traced through the scene using a hybrid path tracing integrator (Algorithm S2). At each diffuse surface intersection \mathbf{x} , we query nearby Gaussians within a radius $r = 0.02$ or $k = 3$ nearest neighbors using a *hybrid radius+kNN* search (Algorithm S3).

Algorithm Algorithm S1. **Stochastic Progressive Photon Mapping (SPPM) baseline** has three stages: (1) photon tracing to build KD-tree, (2) camera pass with KDE-based radiance gathering at first diffuse hits, and (3) progressive radius reduction following $r_{t+1} = r_t \sqrt{\frac{t + \alpha}{t + 1}}$. SPPM is used as a baseline and our ground truth generator (with $T = 1000$ iterations).

```

1 def sppm(scene, camera, light, T, Np, r0=0.02,
2   alpha=0.7):
3   L_accum, rt = 0.0, r0
4   for t in range(T):
5     # 1) Photon tracing: emit Np photons
6     # and build KD-tree
7     P = PHOTON_TRACE(scene, light, Np)
8     # store (pos, flux, wi) on
9     # diffuse surfaces
10    KDT = BUILD_KDTREE(P)
11
12    # 2) Camera pass: first diffuse hit
13    # uses KDE (radius-rt gathering)
14    L_frame = 0.0
15    for pix in camera:
16      ray = PRIMARY_RAY(camera, pix)
17      hit, beta, prev_delta =
18        TRACE_TO_FIRST_DIFFUSE(scene,
19        ray)
20      if hit is None:
21        L_frame += 0.0; continue
22      if prev_delta and IS_EMITTER(hit):
23        L_frame += beta *
24          EMITTER_RADIANCE(hit);
25        continue
26      N = RADIUS_QUERY(KDT, hit.x, rt)
27      Lp = KDE_GATHER(N, hit) # radiance
28      :  $L_p = \frac{1}{\pi r_t^2} \sum \Phi_j f_r$ 
29      L_frame += beta * Lp
30
31    # 3) Progressive radius update
32    rt = r0 * ((t + alpha) / (t + 1))**0.5
33    L_accum += L_frame
34
35 return L_accum / T

```

where w_i is the anisotropic Gaussian weight and $\epsilon = 10^{-6}$ ensures stability. Queries are implemented using a KD-tree structure built from Gaussian centers, rebuilt periodically as positions are optimized.

We only supervise **visible surface points** collected from K camera views ($K = 3-30$ depending on the scene). Each visible point's ground-truth radiance $L_{\text{GT}}(\mathbf{x})$ is obtained from the reference SPPM after 1000 iterations.

We train the field by minimizing the MSE loss

$$\mathcal{L} = \frac{1}{N} \sum_{\mathbf{x}} \|L_{\text{GPF}}(\mathbf{x}) - L_{\text{ref}}(\mathbf{x})\|_2^2, \quad (14)$$

where N is the number of visible surface points, using the Adam optimizer with a learning rate of 5×10^{-4} . Training is performed for 10k iterations, each sampling a random subset of visible points from randomly selected views.

Algorithm Algorithm S2. Camera ray tracing with Gaussian queries. At diffuse surfaces, we query the radiance from GPF, multiply by the BSDF, and terminate. Specular/glossy segments are traced explicitly.

```

1  def render_with_gpf(scene, camera, G, r_query
2      =0.02, k_min=3, kd_tree):
3      """
4          Differentiable camera pass that reuses the
5              learned Gaussian field.
6          Query occurs only at diffuse surfaces;
7              specular/glossy bounces are traced.
8      """
9      L_img = zeros_like(camera.pixels)
10     for pix in camera.pixels:
11         ray = generate_camera_ray(camera, pix)
12         L_pix, beta, prev_delta = 0.0, 1.0,
13             True
14         while True:
15             hit = intersect(ray, scene)
16             if not hit: break
17
18             if is_emitter(hit) and prev_delta:
19                 L_pix += beta *
20                     emitter_radiance(hit, ray.
21                         dir)
22                 break
23
24             wo, fs, pdf, bsdf_type =
25                 sample_bsdf(hit, return_type=
26                     True)
27
28             if is_diffuse(bsdf_type):
29                 # Query learned radiance field
30                     and multiply by BSDF
31                 Li = query_gaussian_radiance(
32                     hit.position, wo, G, kd_tree,
33                     r_query, k_min)
34                 Lg = Li * fs # Apply BSDF
35                     modulation
36                 L_pix += beta * Lg
37                 break # terminate at first
38                     diffuse
39             else:
40                 beta *= fs / pdf
41                 prev_delta = is_delta(
42                     bsdf_type)
43                 ray = spawn_ray(hit, wo)
44
45             L_img[pix] = L_pix
46     return L_img

```

All differentiable operations (Gaussian weighting and gradient accumulation) are implemented in Dr.Jit [17] with full GPU vectorization.

Algorithm Algorithm S3. Hybrid Gaussian radiance query.

We first use a radius query to preserve locality and supplement with kNN to avoid empty neighborhoods. A soft normalization by $\max(\sum w_i, \epsilon)$ ensures stability.

Table S1. **Ablation study on the number of Gaussian primitives.**

# Gaussians	PSNR↑	SSIM↑	LPIPS↓	Time (s)↓
10K	24.32	0.8521	0.2847	7.230
50K	26.18	0.8892	0.2156	12.70
100K	27.12	0.9355	0.1579	16.37
200K	27.25	0.9403	0.1564	24.35

```

1  def query_gaussian_radiance(x, view_dir, G,
2      kd_tree, r=0.02, k_min=3, eps=1e-6):
3      """
4          x: surface point (query)
5          view_dir: outgoing direction (to camera)
6          G: Gaussian params [(mu, sigma,
7              quat, color), ...]
8          kd_tree: built over {mu}
9          r: radius for ball query (default:
10              0.02)
11         k_min: minimal neighbors guaranteed by
12             kNN supplement (default: 3)
13         returns: radiance estimate at x
14     """
15
16     # Phase 1: radius query
17     idx_r = kd_tree.ball_query(x, r)
18
19     # Phase 2: supplement with kNN if sparse
20     if len(idx_r) < k_min:
21         idx_knn = kd_tree.knn_query(x, k_min)
22         idx = dedup(idx_r + idx_knn)
23     else:
24         idx = idx_r
25
26     # Phase 3: accumulate weighted
27         contributions
28     L = 0.0
29     Z = 0.0
30     for j in idx:
31         mu, sigma, quat, color = G[j]
32         R = quat_to_matrix(quat)
33             # 3x3 rotation
34         d = x - mu
35         dL = R.T @ d # to local frame
36         dn = (dL[0]/sigma[0], dL[1]/sigma[1],
37             dL[2]/sigma[2])
38         w_gauss = exp(-0.5 * dot(dn, dn))
39             # anisotropic kernel
40             # soft distance falloff (smooth
41                 outside r)
42         dist = norm(d)
43         if dist <= r:
44             w_dist = 1.0
45         else:
46             t = (dist - r) / max(r, 1e-6)
47             w_dist = exp(-3.0 * t * t)
48             w = w_gauss * w_dist
49             L += color * w
50             Z += w
51
52     return L / max(Z, eps)

```

B. Ablation Study

Ablation on Different Number of Gaussian Primitives.

Table S1 investigates the effect of varying the number of Gaussian primitives. Increasing the number of Gaussians

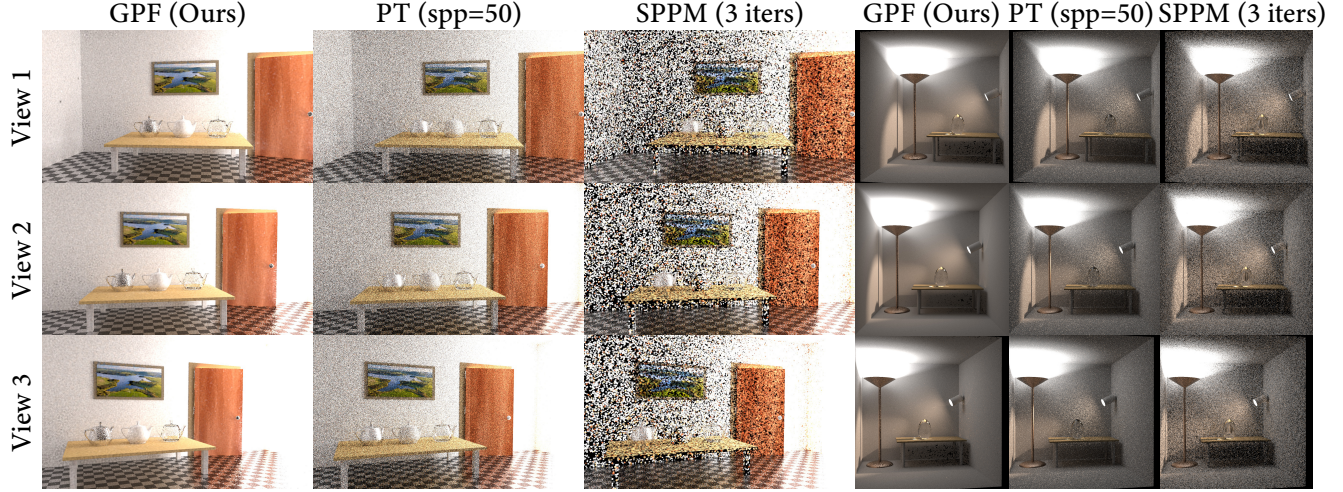


Figure S1. **Multi-view rendering results.** We compare our solution with *Mitsuba 3 Path Tracer* [16], *SPPM* [12], *3DGS* [22] and *Instant-NGP* [29] across water-caustic. Our method produces cleaner results with significantly fewer noise artifacts and more accurate light transport, especially in challenging caustic. Please zoom in for more details.

Table S2. **Ablation study on the k-NN parameter k .**

k	PSNR \uparrow	SSIM \uparrow	LPIPS \downarrow	Time (s) \downarrow
1	25.87	0.8756	0.2314	16.21
3	27.12	0.9355	0.1579	16.37
5	27.18	0.9372	0.1574	16.48
10	27.08	0.9342	0.1595	16.34

consistently improves image quality, as reflected by higher PSNR/SSIM and lower LPIPS, owing to denser photon coverage and finer radiance approximation. However, beyond 100K primitives, the performance gain becomes marginal while rendering time increases notably. We therefore adopt 100K Gaussians as a balanced configuration between quality and efficiency.

Ablation on Different k-NN Parameter. Table S2 analyzes the influence of the k -nearest-neighbor parameter on radiance aggregation. A too small k (e.g., $k=1$) leads to unstable estimation and higher noise due to insufficient photon support, while an excessively large k oversmooths high-frequency lighting and caustic details. The overall performance remains stable for k between 3 and 5, showing nearly identical image quality and computation time. We adopt $k=3$ as our default setting for its robustness and simplicity.

C. Additional Experiment Results

We also provide a supplementary video demonstrating the multi-view rendering consistency across all scenes.

Multi-View Rendering Results on Veach-Ajar and Veach-Bidir. We present multi-view rendering results on the *Veach-Ajar* and *Veach-Bidir* scenes from three viewpoints (Figure S1). Our method is compared with Path Tracing (50 spp) and SPPM (3 iterations). The results demon-

strate that our approach produces cleaner images with reduced noise and more stable indirect illumination across views compared to both baselines.

Multi-View Rendering Results on Water-Caustic. We present multi-view rendering results on the *Water-Caustic* (Figure S2) scene using four viewpoints. We compare our method with 3DGS under both *3-view* and *10-view* supervision, as well as with Path Tracing (50 spp) and SPPM (3 iterations). The results indicate that our method achieves sharper caustic structures, reduced noise levels, and more stable multi-view radiance behavior compared to the baseline approaches.

Multi-View Rendering Results on Water-Caustic 2. We present multi-view rendering results on the *Water-Caustic 2* scene (Figure S3), using four viewpoints. We compare our method with 3DGS and Instant-NGP under both *3-view* and *10-view* supervision, as well as with Path Tracing (50 spp) and SPPM (3 iterations). The results show that our approach produces cleaner caustics, fewer noise artifacts, and more consistent light transport across views compared to all baselines.

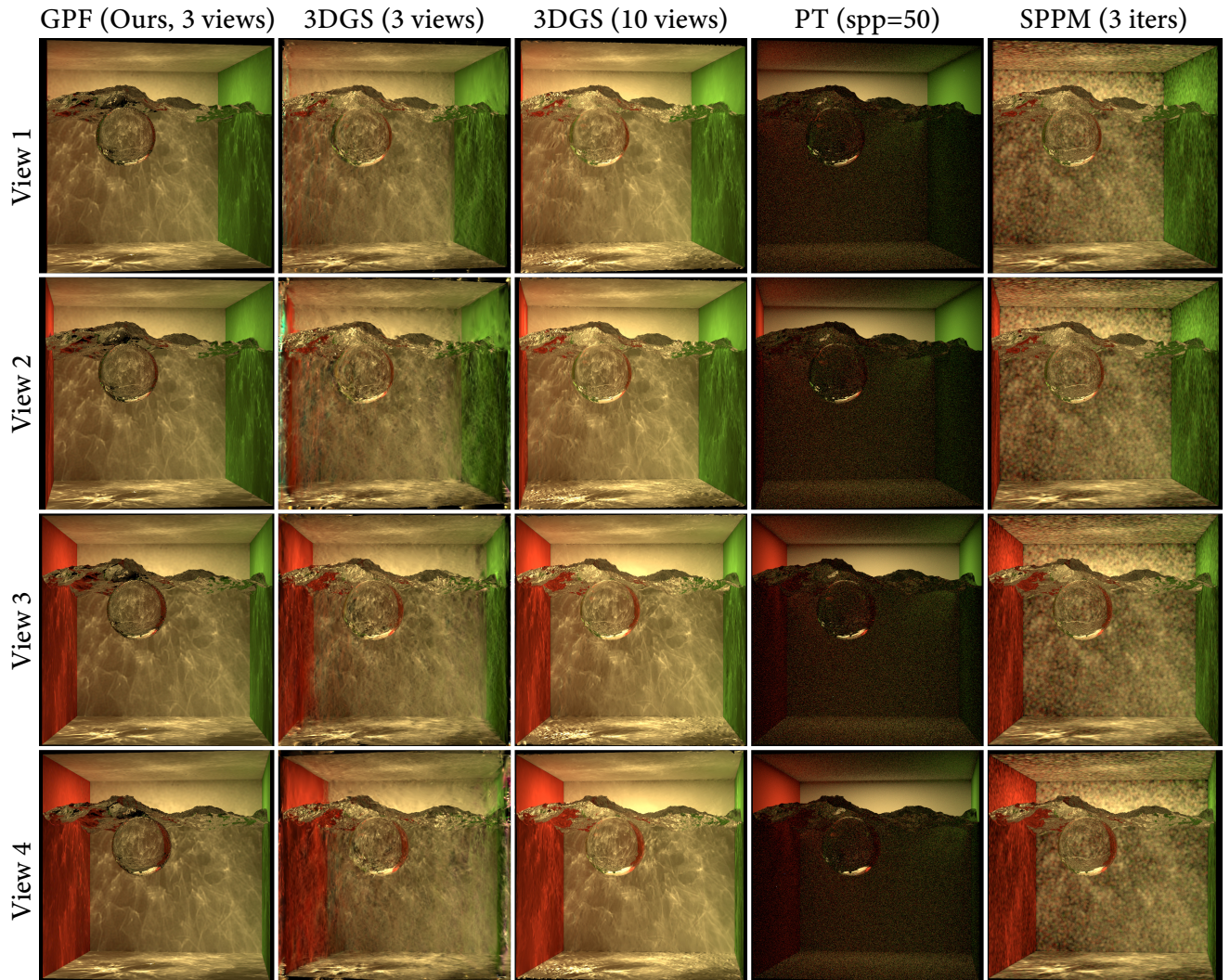


Figure S2. **Multi-view rendering results.** We compare our solution with *Mitsuba 3 Path Tracer* [16], *SPPM* [12], *3DGS* [22] across water-caustic. Our method produces cleaner results with significantly fewer noise artifacts and more accurate light transport, especially in challenging caustic. Please  zoom in for more details.

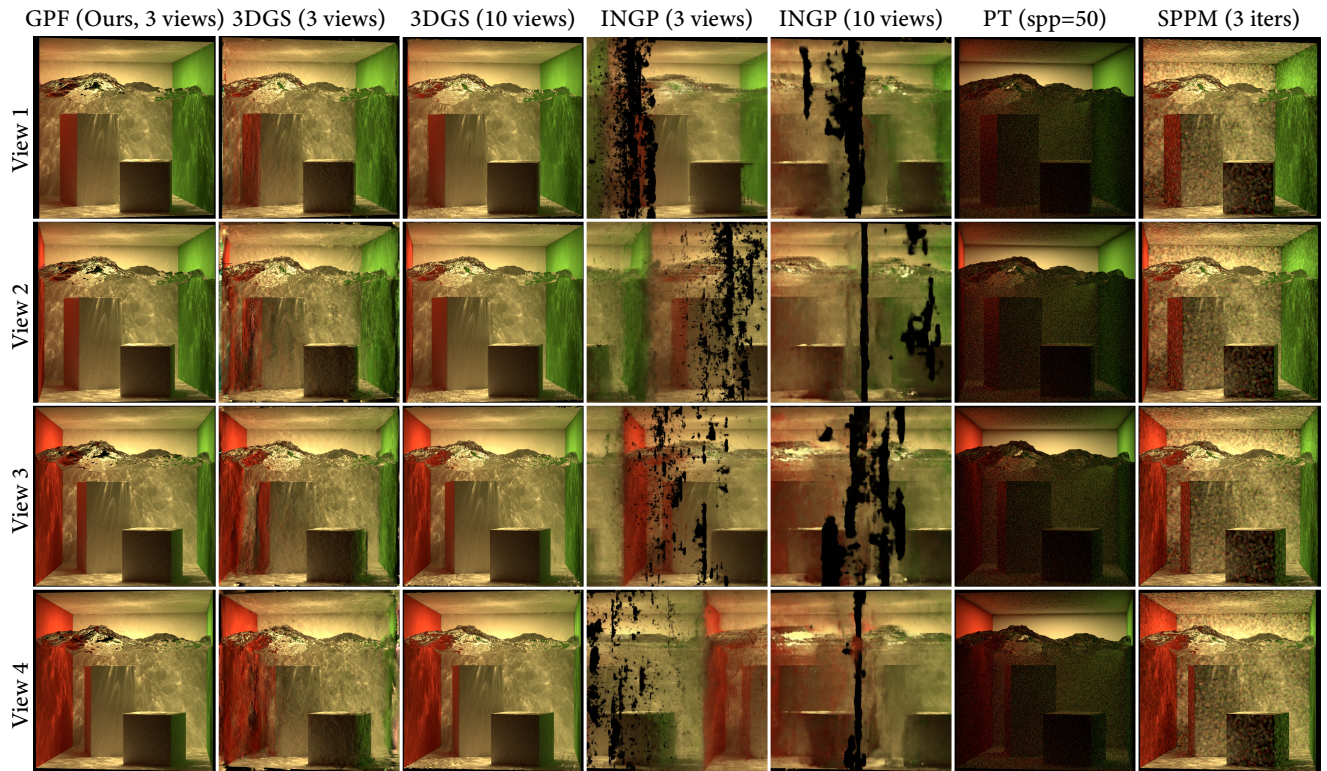


Figure S3. **Multi-view rendering results.** We compare our solution with *Mitsuba 3 Path Tracer* [16], *SPPM* [12], *3DGS* [22] and *Instant-NGP* [29] across water-caustic. Our method produces cleaner results with significantly fewer noise artifacts and more accurate light transport, especially in challenging caustic. Please zoom in for more details.